ACS Energy LETTERS

http://pubs.acs.org/journal/aelccp

Acidic Electroreduction of CO_2 to Multi-Carbon Products with CO_2 Recovery and Recycling from Carbonate

Alessandro Perazio, Charles E. Creissen,* José Guillermo Rivera de la Cruz, Moritz W. Schreiber, and Marc Fontecave*

Cite This: *ACS Energy Lett.* 2023, 8, 2979–2985 Read Online

ACCESS | Metrics & More | Article Recommendations | Supporting Information

ABSTRACT: **Gas-fed flow cells can facilitate high-rate electrochemical CO_2 reduction (CO_2R). However, under alkaline and neutral conditions, CO_2 is lost through reaction with hydroxide ions to form (bi)carbonate. In acidic solutions, although (bi)carbonate is still formed due to increased pH at the electrode, the low bulk pH of the electrolyte solution can regenerate CO_2 which is then available for re-reaction or release—this therefore avoids permanent CO_2 loss. Here, we show how CO_2 is converted and released in a bipolar-membrane-based gas-fed flow cell for CO_2R to multicarbon products (C_{2+} faradaic efficiency >60%) employing an acidic catholyte. Under the highest conversion conditions, we showed that almost exclusively CO_2R products were obtained at one outlet, while, at the second outlet, a nearly product-free stream of CO_2 was obtained due to the continuous internal regeneration from (bi)carbonate. The system presented here avoids permanent reactant loss through the straightforward recovery and recycling of CO_2 to improve the overall CO_2 utilization.**

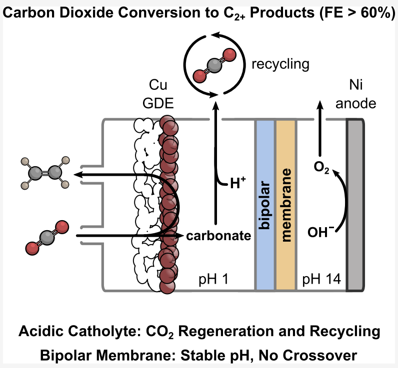

Electrochemical CO_2 reduction (CO_2R) offers a sustainable route to generate valuable chemical products from CO_2 and renewable electricity sources.[1,2] Recent progress has brought CO_2R closer to commercial viability through the development of devices that overcome the severe limitations of mass transport arising from the low solubility of CO_2 in aqueous solutions. One example is the gas-fed flow cell, in which the CO_2 is supplied as a gas through the back of a gas-diffusion electrode (GDE) in contact with a flowing electrolyte solution—these devices can regularly attain high current densities (hundreds of mA cm^{-2}) at low overpotentials (<1 V).[3−7] However, the common use of alkaline or neutral pH electrolyte solutions has prohibited high conversion yields due to the unwanted reaction of CO_2 with hydroxide ions, which results in reactant loss through the formation of (bi)carbonate (Figure 1a).[8,9] These species can be externally converted back to CO_2, but the regeneration process accounts for more than half of the energy required for the electrolyzer in the case of an alkaline flow-cell.[10] The problem can be partly addressed by using acidic electrolyte solutions where the pH is below the pK_a of bicarbonate formation.[11−13] In such systems, while the CO_2 is still converted to (bi)carbonate at high current densities (eqs 1 and 2) by the alkaline local pH at the cathode arising from hydroxide ions generated during CO_2 reduction (eq 3),[12,14] these species are immediately converted back to CO_2 (here termed r-CO_2 as this is regenerated) due to the low bulk pH (eqs 4 and 5, Figure 1b).

$$CO_2 + OH^- \rightleftharpoons HCO_3^- \tag{1}$$

$$HCO_3^- + OH^- \rightleftharpoons CO_3^{2-} + H_2O \tag{2}$$

$$CO_2 + H_2O + 2e^- \rightleftharpoons CO + 2OH^- \tag{3}$$

$$HCO_3^- + H^+ \rightleftharpoons \text{r-}CO_2 + H_2O \tag{4}$$

$$CO_3^{2-} + 2H^+ \rightleftharpoons \text{r-}CO_2 + H_2O \tag{5}$$

We sought to understand the generation and transport of r-CO_2 in a gas-fed flow cell for CO_2R to multicarbon (C_{2+}) products by analyzing the compositions of the different gas outlets. Here, we show that carbonate species are completely reconverted to r-CO_2 with high purity, which exits from a first outlet (indirect outlet) where it is mixed with the flowing catholyte, while concentrated gas products are obtained at a

Received: May 5, 2023
Accepted: June 1, 2023
Published: June 26, 2023

https://doi.org/10.1021/acsenergylett.3c00901
ACS Energy Lett. 2023, 8, 2979–2985

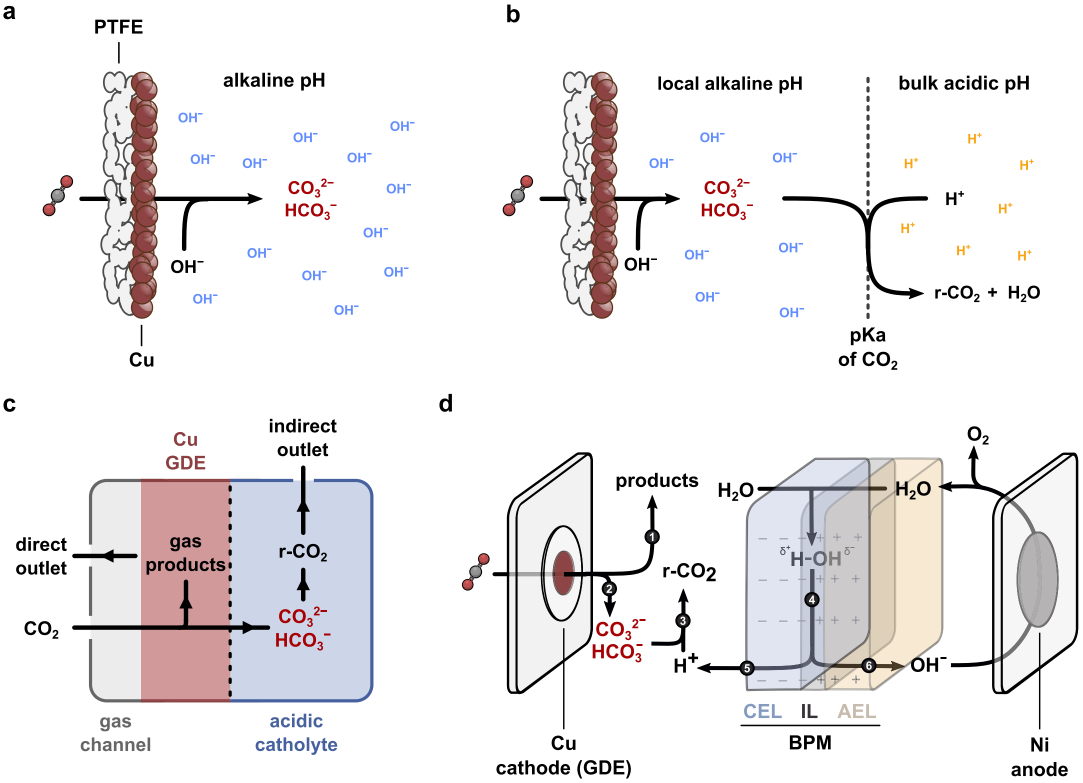

Figure 1. Schematic representation of electrolyte effects and the reactor setup. (a) A Cu gas-diffusion cathode interfaced with an alkaline bulk pH electrolyte, in which (bi)carbonate species accumulate in solution. (b) A Cu cathode interfaced with an acid bulk pH electrolyte, in which (bi)carbonate species are formed and then converted back to r-CO_2 by protonation in the bulk solution. (c) Schematic showing how r-CO_2 is preferentially released from the indirect outlet while gas products are collected mainly from the direct outlet. (d) The full-cell assembly with a BPM, where (1) CO_2 is reduced to products, (2) CO_2 is converted to (bi)carbonate, (3) CO_2 is regenerated, (4) H_2O dissociates in the BPM interlayer, (5) protons diffuse through the cation exchange layer (CEL) into the catholyte, and (6) hydroxide ions diffuse through the anion exchange layer (AEL) into the anolyte.

second outlet (direct outlet) positioned at the back of the GDE (Figure 1c). This elegant solution avoids CO_2/product separation and enables recycling and re-reaction of the r-CO_2, which maximizes the overall CO_2 utilization since a higher proportion of the supplied CO_2 is ultimately converted into reduction products and is not permanently lost as (bi)carbonate.

The electrolyzer we employed for CO_2R to C_{2+} products incorporated a CO_2-fed gas-diffusion electrode (GDE) with a Cu catalyst, which was interfaced with flowing acidic catholyte (Figure 1d, Figure S1). The anode choice for the cell is important as it also dictates the type of membrane that can be used. So far, all existing CO_2R devices with flowing acidic catholyte have employed cation exchange membranes (CEMs), which require acidic anolyte solution.[11−13] These systems use acid-stable OER catalysts which contain expensive precious metals such as Ir or Ru, the cost of which has been identified as a barrier to device upscaling in water electrolyzers and therefore could also prove problematic for CO_2R devices.[15] Bipolar membranes (BPMs) avoid this issue as they enable alkaline anolyte to be used with acidic catholyte, as the water dissociation reaction occurring at the interlayer maintains a pH gradient (Figure 1d).[16,17] Although BPMs add an additional voltage penalty, they enable the use of Earth-abundant catalysts, which has been demonstrated in alkaline and neutral flow cells[18−20] and membrane electrode assemblies[21,22] but until now has not been demonstrated under acidic catholyte conditions which avoid CO_2 loss. The additional benefit is that BPMs prevent crossover of metal ions and cationic electrolyte species, which can negatively impact device performance and long-term stability when CEMs are used.[17,23] Here, we used a BPM with a Ni foam anode to enable independent evaluation of the cathode compartment and to highlight some advantages of such configurations.

We used a Cu catalyst, obtained through electroreduction of a CuO precatalyst which was synthesized using a simple solvothermal procedure.[24] In brief, a solution of Cu(acetate)$_2$ in ethanol was heated to 200 °C in an autoclave for 20 h to obtain nanoparticles approximately 50 nm in size (Figure S2). X-ray diffraction (XRD) patterns displayed peaks corresponding to pure CuO (Figure S3). GDEs were formed by spray-coating a methanolic solution containing the as-prepared CuO nanoparticles and Nafion onto a polytetrafluoroethylene (PTFE) membrane to reach a loading of 2 mg cm^{-2}, corresponding to an approximate thickness of 6 μm (Figure S4). An activation step was required to obtain metallic Cu, the active catalyst, from the initial oxide. This involved running consecutive linear sweep voltammograms (LSVs) from −0.5 to −1.9 V vs Ag/AgCl until the current response was constant, followed by chronopotentiometry (CP) at −200 mA cm^{-2} for 1 h using a 3 M KCl solution as the catholyte. The metallic nature of the catalyst was confirmed by XRD (Figure S3). These activated Cu-GDEs were used for all experiments.

The same anolyte (2.5 M KOH, pH 14) was used throughout all experiments with a nickel foam anode—only the catholyte composition was varied. We initially chose 0.5 M

https://doi.org/10.1021/acsenergylett.3c00901
ACS Energy Lett. 2023, 8, 2979−2985

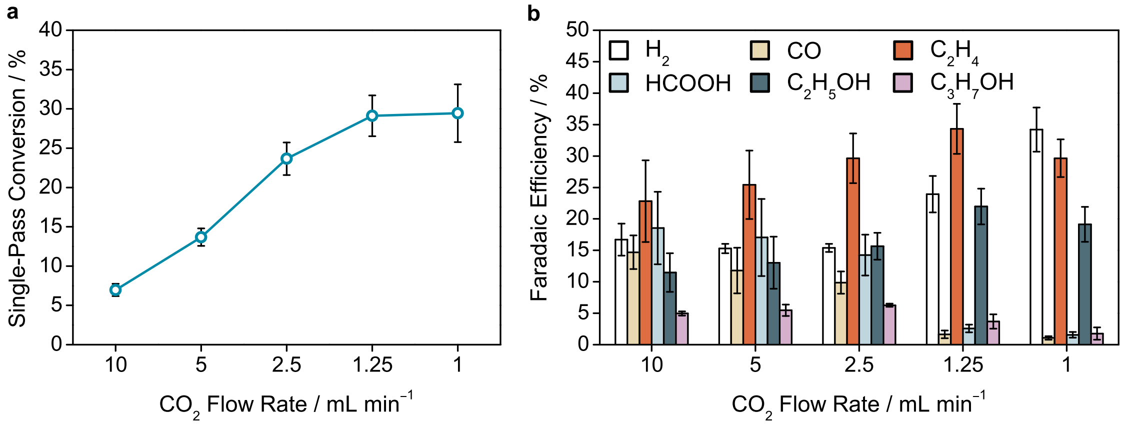

Figure 2. Effects of altering the CO_2 flow rate on (a) single-pass conversion and (b) selectivity. The data were obtained after performing each electrolysis for 30 min at −200 mA cm^{-2} with a 0.05 M H_2SO_4 + 3 M KCl catholyte. The error bars represent the standard deviation from the mean for three different electrodes.

KH_2PO_4 with 2 M KCl (pH 4) as the catholyte because of its good buffering properties; however, we observed deterioration of the initially high C_{2+} product selectivity over time (Figure S5). We speculate that the phosphate species could chelate to Cu and alter the surface structure over time; however, validation of this requires further investigation which is beyond the scope of this research. As the use of sulfate anions did not result in loss of C_{2+} selectivity, we replaced phosphate with a low concentration of H_2SO_4 (0.05 M, pH 1) and explored effects arising from the addition of varying amounts of KCl. As with previous reports, the addition of KCl improved selectivity by limiting H_2 evolution (Figure S6).[11,13,25,26] Even though 0.5 M KCl was sufficient to prevent significant H_2 evolution, the greater conductivity provided by higher concentrations reduced the solution resistance, thereby lowering the full cell potential (Figure S6). With 3 M KCl, a high C_{2+} product selectivity (52%) and a relatively low cell potential (−4.7 V at −200 mA cm^{-2}) were achieved. Using this optimized setup, we aimed to enhance conversion.

We initially sought to achieve the maximum conversion of CO_2 to CO_2R products in the acidic catholyte system. To evaluate this, we used a parameter termed the single-pass CO_2 conversion to CO_2R products (SPC), which describes the yield of CO_2R products with respect to the amount of CO_2 supplied (eq 6).

$$\text{SPC (\%)} = \sum \left\{ \left[\left(\frac{j_{\text{product}} \times 60\text{ s}}{n_{\text{electrons}} \times F} \right) \div \left(\frac{\text{flow rate}}{24.05} \right) \right] \times \text{carbon atoms} \times 100 \right\} \tag{6}$$

To obtain the total SPC, the single pass conversion values for each carbon product are summed. In eq 5, j_{product} is the partial current density (mA cm^{-2}) for a specific product, $n_{\text{electrons}}$ is the number of electrons needed for its production, F is the Faraday constant, the flow rate is the one chosen for the feed CO_2 (mL min^{-1}), and 24.05 is the molar volume of a gas (L) at normal temperature and pressure. Several factors can alter the SPC, including the reaction rate, the flow rate of CO_2, and the type and amount of products generated. This is because the product influences the amount of hydroxide ions formed, which in turn will determine how much CO_2 is converted to transient (bi)carbonate species. For example, in the case of a catalyst selective only toward ethylene, 12 OH^- are generated per molecule of ethylene formed, resulting in a maximum SPC of only 25% if there is no possibility for the r-CO_2 to re-react. Similarly, the maximum SPC is 50% in the case of a catalyst selective for CO, which involves the generation of two OH^-. Overcoming the limits imposed for a specific product distribution (and the resulting hydroxide formation) would require re-reaction of r-CO_2 to counteract the conversion losses arising from (bi)carbonate formation. In addition we define a CO_2 utilization which is the ratio of CO_2 used for reaction to the CO_2 available, calculated according to eq 7, in which $\dot{n}_{CO_2\,\text{total}}$ (nmol s^{-1}) is the molar flow of CO_2 available for reaction (including r-CO_2 in the case of recycling) and $\dot{n}_{CO_2\,\text{unused}}$ (nmol s^{-1}) is the molar flow of CO_2 which does not contribute to products and is vented from the system. The utilization is equivalent to the SPC for a system that does not recycle the r-CO_2.

$$\text{utilization (\%)} = \frac{\dot{n}_{CO_2\,\text{total}} - \dot{n}_{CO_2\,\text{unused}}}{\dot{n}_{CO_2\,\text{total}}} \times 100 \tag{7}$$

We optimized the single-pass conversion to CO_2R products of our system by altering the CO_2 feed flow rate at a fixed current density of −200 mA cm^{-2}. As expected, decreasing the flow rate from 10 to 1.25 mL min^{-1} increased the SPC to reach a value of (29 ± 3)% at 1.25 mL min^{-1} (Figure 2a). This is because a higher proportion of the CO_2 fed into the system is reacting at lower flow rates. However, lowering the flow rate to 1 mL min^{-1} did not lead to a higher SPC, as the production of hydrogen increased at the expense of CO_2R products—this caused the SPC to plateau at 29% as a consequence of the low availability of CO_2 for reaction at the catalyst surface (Figure 2b and Figure S7). For a given product distribution at a set rate of reaction (current density), lowering the flow rate should increase the SPC. Here, as H_2 production increased at 1 mL min^{-1}, this suggested that nearly all CO_2 was converted either to CO_2R products or (bi)carbonate, resulting in the surplus current being used to reduce water to H_2. The only way this excess H_2 evolution could have been avoided was if re-reaction of r-CO_2 was possible, or if there was a lower degree of (bi)carbonate formation, both of which would result in increased CO_2 availability at the cathode and therefore higher CO_2R selectivity and SPC. Therefore, our experimental data suggested that re-reaction of r-CO_2 was not dominant in this setup—this is further supported and described in the analysis of the composition of the gas outlets below.

We observed an interesting dependence of selectivity on the CO_2 flow rate. When decreasing the flow rate, we noticed an increase in selectivity for C_{2+} products with a concomitant decrease in C_1 selectivity (Figure 2b, Table S1). The highest FEs for ethylene, (34 ± 4)%, and ethanol, (22 ± 3)%, were obtained at 1.25 mL min^{-1}. To help rationalize this, we plotted the CO_2, CO, and C_2H_4 concentrations as a function of conversion (Figure S8). The trend showed that, as conversion increased, the concentration of CO decreased while the concentration of C_2H_4 increased. This concentration profile is typical for a series reaction and is in line with the conversion of CO_2 to C_2 products via CO as an intermediate.[27] An additional factor to consider when varying the reactant CO_2 flow rate is the compromise between conversion and productivity, which is defined as the amount of CO_2 reduced to CO_2R products per minute for a given geometric catalyst area.[28] Our results showed that the productivity decreased with increasing SPC (Figure S9), in accordance with previous reports.[29,30] This consideration identifies an optimal feed flow rate for a CO_2R electrolyzer to target a specific productivity-conversion point, and therefore, reaching a maximum SPC is not always the best option if productivity is significantly lowered. Such evaluation will become increasingly important as CO_2R progresses toward commercialization.

We assessed the ability of the electrolyzer to operate at its highest conversion point over extended periods (Figure 3). Over 8 h, the FEs for CO_2R products were stable (Figure 3a, Table S2) and, through analysis of liquid samples from the anolyte using ^1H NMR, we confirmed that there was no product crossover between the cell compartments. Additionally, we showed that a stable catholyte pH could be maintained for the duration of the experiment with an alkaline anolyte (Figure 3b). We also used inductively coupled plasma-mass spectroscopy (ICP-MS) to detect any crossover of K^+ and observed that there was no significant shift in K^+ concentration on either side of the cell (Figure 3c). The system maintained a full-cell potential (E_{cell}) of −5.4 V with an average SPC of 26% toward CO_2R products (Figure S10). We additionally compared the BPM system with an equivalent setup using a CEM and acidic anolyte with an IrO_x anode (Figure S11). The cathode was identical in each case and therefore the same process of regeneration took place in this compartment, but the voltage of the CEM system ($|E_{cell}|$ = 3.8 V) was lower than the corresponding BPM system ($|E_{cell}|$ = 4.7 V). This large voltage penalty of BPMs is due to the process of water dissociation at the interlayer, for which most commercially available BPMs typically exhibit a large overpotential, as well as additional Ohmic losses from resistive components.[31] However, the ability to use Earth-abundant OER catalysts with alkaline conditions makes BPMs attractive components for CO_2R. Recent developments of catalyst-loaded BPMs have shown a significant reduction in the overpotential for water dissociation, which could enhance performance to limit voltage penalties in the near future.[32−34]

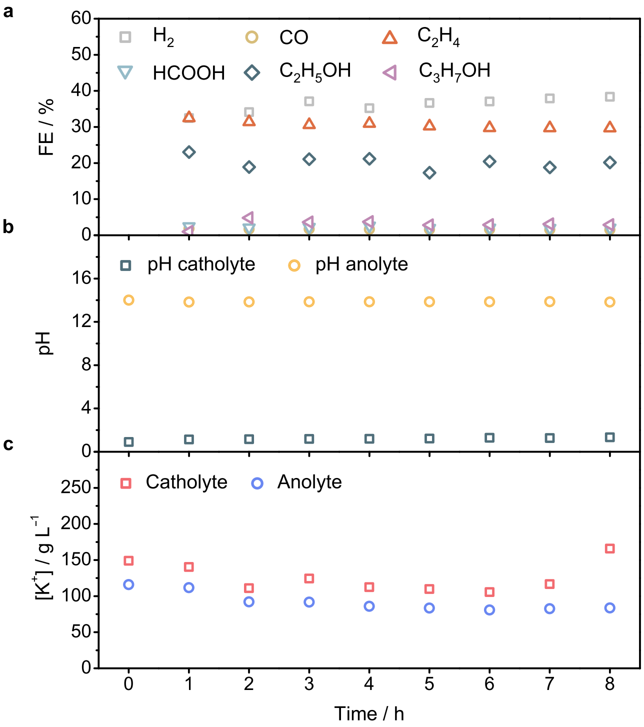

Figure 3. Stability test performed at −200 mA cm^{-2} with a feed CO_2 flow rate of 1.25 mL min^{-1} and a 0.05 M H_2SO_4 + 3 M KCl catholyte solution. (a) FE changes for each product over time. (b) pH stability over time. (c) K^+ concentration in each compartment over the duration of electrolysis analyzed using ICP-MS.

Having established a highly robust system that could operate at high conversion over extended periods, we looked to better understand the different routes through which the feed CO_2 and r-CO_2 are reacted and/or vented from the device. Previous reports using acidic catholytes have suggested that re-reaction of r-CO_2 can occur to boost the SPC.[11] However, in our case the experimental data showed that re-reaction of r-CO_2 is not dominant, as the SPC plateaus at lower flow rates. To estimate the pH and resulting CO_2 concentration profiles under reaction conditions, we constructed a one-dimensional diffusion−reaction model based on previous reports (details provided in the Supporting Information).[11−13] The results showed that the high alkalinity at the electrode is responsible for the (bi)carbonate formation but that regeneration occurs within 35 μm from the surface (Figure S12). Although diffusion of r-CO_2 back toward the surface for re-reaction should be possible, it is competitive with reaction with OH^- to form (bi)carbonate. As the OH^- exists in high concentrations close to the electrode surface, we postulated that r-CO_2 was more likely to degas through the catholyte solution instead. Considering this observation, we aimed to develop a more complete picture of the CO_2 conversion efficiency of the system and focused on recovery of the CO_2 regenerated from carbonate species. We developed a series of experiments to understand these processes through analysis of the composition of the gas outlets of the reactor.

There are two gas outlets in our device. The first one is positioned at the back of the GDE and is identified as the direct outlet, which collects unreacted CO_2 and gas products. The second gas outlet is located on the side of the reactor, contained within the flowing catholyte solution, and is termed as the indirect outlet—this collects the r-CO_2 and gas products that degas from the electrolyte solution (Figure 4a and Scheme S1). We analyzed the composition of the gas streams vented from each outlet under the CO_2R conditions used in our stable system as well as under zero-current conditions.

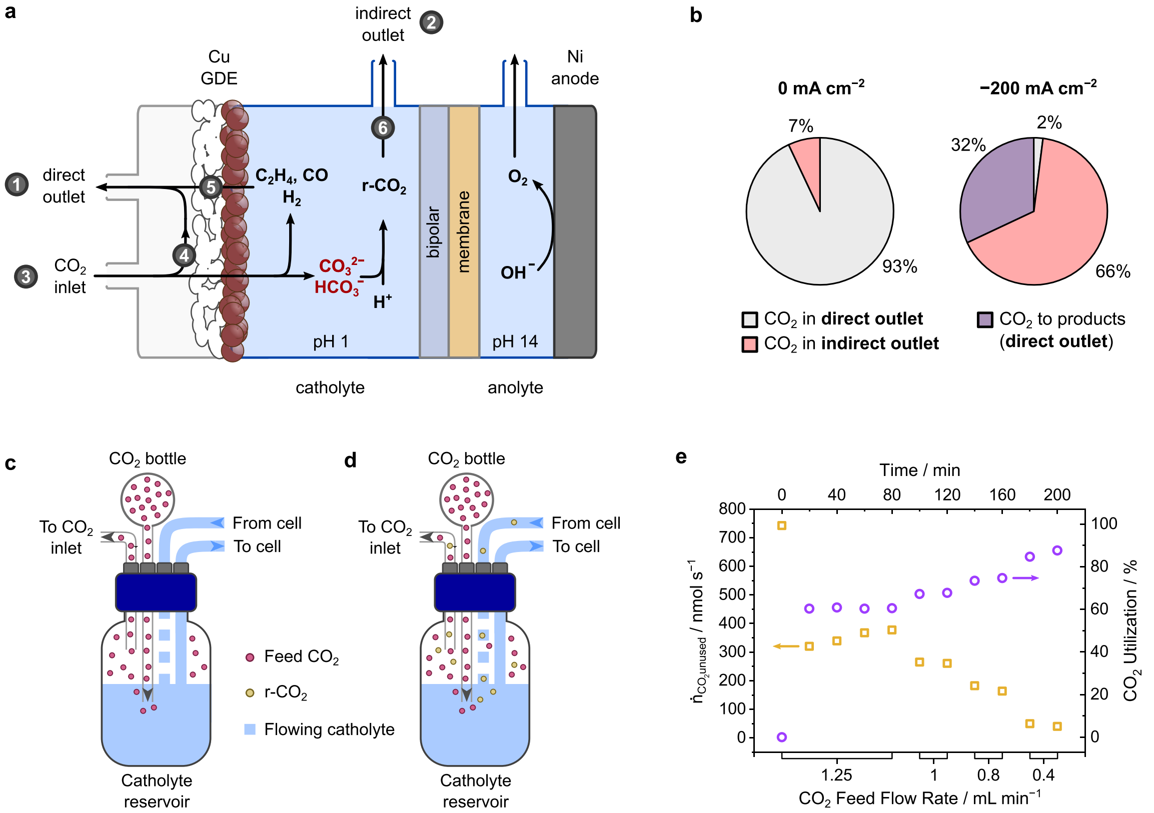

Figure 4. (a) Schematic representation of the full cell (cross section) showing the outlets of the reactor, with the different pathways for the feed CO_2: (1) direct outlet, (2) indirect outlet, (3) CO_2 inlet, (4) CO_2 that bypasses the cell without crossing the GDE, (5) products release, (6) r-CO_2 release. (b) The CO_2 distribution under working and idle conditions. When no current is applied, most of the feed CO_2 can be found at the direct outlet, while during electrolysis the majority is collected from the indirect stream as r-CO_2. Conditions: 30 min electrolysis, CO_2 flow rate of 1.25 mL min^{-1}, electrolyte solution of 0.05 M H_2SO_4 + 3 M KCl. (c) CO_2 pathway inside the catholyte reservoir in the recycling configuration when $j = 0$ mA cm^{-2} and (d) when $j = -200$ mA cm^{-2}. (e) Results of the recycling test: the CO_2 molar flow leaving the cell through the direct outlet (yellow squares) and the CO_2 utilization (purple circles) were monitored over time during electrolysis at −200 mA cm^{-2} with the recycling configuration.

First, we checked the amount of CO_2 passing through each outlet under idle conditions (0 mA cm^{-2}) and under catalytic conditions (−200 mA cm^{-2}) while keeping the feed CO_2 flow rate constant at 1.25 mL min^{-1} (Figure 4b, Table S3). In both cases, the total combined amount of CO_2 and CO_2R products was the same, therefore providing a closed carbon mass balance. With no current, the majority of the feed CO_2 was retrieved at the direct outlet (93%). In contrast, under catalytic conditions, only a small fraction of CO_2 was obtained at the direct outlet (2%), showing that reactant bypassing of the cell was low, while the remainder of the CO_2 was recovered at the indirect outlet (66%). This distribution shows that, during electrolysis, almost all of the feed CO_2 crosses the GDE and is converted to either carbonate species or reduction products, which account for a CO_2 utilization of 32% of the feed CO_2 corresponding well with the obtained SPC value. The (bi)carbonate species are neutralized by the acidic bulk electrolyte solution to generate r-CO_2, which vents preferentially through the indirect outlet. The composition of both streams showed that all the carbon gas products are obtained at the direct outlet, while the liquid products accumulate in the catholyte and only small quantities of hydrogen are seen in the indirect outlet stream alongside the r-CO_2 (Figure S13). In addition, we showed that it was possible to directly recycle and re-react the almost pure r-CO_2 stream from the indirect outlet by modifying the configuration of the setup (Scheme S2). With no applied current, the feed CO_2 flows into the catholyte reservoir to saturate the headspace, before being injected into the reactor through the CO_2 inlet (Figure 4c). When current is applied, r-CO_2 is generated, which mixes with the feed CO_2 in the catholyte reservoir before injection through the CO_2 inlet (Figure 4d). We monitored the CO_2 utilization as a function of the feed flow rate (Figure 4e). The initial point (time = 0) was measured after saturation of the system with no applied current, with a feed flow rate of 1.25 mL min^{-1}. Under these constant feed flow rate conditions when a current was applied, the $\dot{n}_{CO_2\,total}$ increased due to addition of r-CO_2 to the feed CO_2, but $\dot{n}_{CO_2\,unused}$ also increased as the conversion to products was constant—this resulted in a constant CO_2 utilization of ∼60%. Importantly, as the feed CO_2 flow rate was lowered, the $\dot{n}_{CO_2\,unused}$ decreased, leading to an increase in the CO_2 utilization. This meant we were able to push the system past the previous limit of 1.25 mL min^{-1} shown in Figure 2 without losing selectivity (shown in Figure S14) due to the additional CO_2 flow provided by the r-CO_2, which maintained a constant effective inlet flow rate of CO_2 for reaction. We reached a CO_2 utilization of 88% with a feed flow rate of 0.4 mL min^{-1}, demonstrating that r-CO_2 recycling could be used to increase the overall utilization of CO_2. A proposed scheme showing how this would work in a larger system with a flow rate feedback loop is displayed in Figure

S15. This solution elegantly avoids downstream CO_2/product separation through processes such as amine-based capture, which typically dominates the energy consumption of the product purification.[35] As devices move toward operation at high conversions, cell modifications to improve gas management, CO_2 recovery, and recycling will become more important. Here we showed that, in this cell design and setup, independent of the membrane used, the CO_2 could be recovered. Furthermore, even with nonunity single-pass conversion, the overall utilization of CO_2 could be maximized through recycling of r-CO_2 and flow rate modulation, reducing the need for downstream separation.

The acidic CO_2R system we presented here displayed a high C_{2+} selectivity with continuous internal CO_2 regeneration and recycling. In this first reported example of CO_2R with a flowing acidic catholyte using a bipolar membrane, we showed that crossover of products or contaminants could be avoided and that the electrolyzer maintained a pH gradient with acidic catholyte and alkaline anolyte. With low flow rates of CO_2 at the cathode, the selectivity for C_{2+} products was above 60%, leading to a single-pass conversion efficiency to CO_2R products of (29 ± 3)%. Importantly, the CO_2 regenerated from (bi)carbonate (r-CO_2) could be recovered as an almost product-free stream at the indirect outlet and effectively recycled to achieve high overall utilization (>85%), with an almost pure product stream being obtained at the direct outlet. The internal regeneration and recovery process avoids energy-intensive and expensive separation procedures without impacting the reactor performance, and we envisage that these observations will prove useful in the future development of CO_2R reactors.

ASSOCIATED CONTENT

Supporting Information

The Supporting Information is available free of charge at https://pubs.acs.org/doi/10.1021/acsenergylett.3c00901.

> Experimental methods; Cu nanoparticle synthesis and electrode preparation; gas and liquid product analysis; depiction of the full setup; electrolyte effects; productivity and single-pass conversion trade-off; direct and indirect outlet stream composition; Faradaic efficiencies and SPC values of flow test and long-term experiment; and 1D model methods and results (PDF)

AUTHOR INFORMATION

Corresponding Authors

Charles E. Creissen – *School of Chemical and Physical Sciences, Keele University, Staffordshire ST5 5BG, U.K.;* orcid.org/0000-0002-2144-7261; Email: c.e.creissen@keele.ac.uk

Marc Fontecave – *Laboratoire de Chimie des Processus Biologiques, CNRS UMR 8229, Collège de France, 75231 Paris, France;* orcid.org/0000-0002-8016-4747; Email: marc.fontecave@college-de-france.fr

Authors

Alessandro Perazio – *Laboratoire de Chimie des Processus Biologiques, CNRS UMR 8229, Collège de France, 75231 Paris, France*

José Guillermo Rivera de la Cruz – *Laboratoire de Chimie des Processus Biologiques, CNRS UMR 8229, Collège de France, 75231 Paris, France*

Moritz W. Schreiber – *Total Research and Technology, Refining and Chemicals, Division CO_2 Conversion, Feluy 7181 Seneffe, Belgium*

Complete contact information is available at: https://pubs.acs.org/10.1021/acsenergylett.3c00901

Author Contributions

Conceptualization: A.P., C.E.C., and M.F. Methodology: A.P., C.E.C., and M.F. Investigation: A.P. and C.E.C. Writing−original draft: A.P., C.E.C., and M.F. Writing−review and editing: A.P., C.E.C., J.G.R.d.l.C., M.W.S., and M.F. Funding acquisition: M.F. and M.W.S. Supervision: C.E.C. and M.F.

Notes

The authors declare the following competing financial interest(s): A provisional European patent application for this work was filed on the 13th of October 2022 in the joint names of TotalSE and Collège de France.

ACKNOWLEDGMENTS

This work was supported financially by funding from Total Research & Technology Feluy. We thank Françoise Pillier for SEM analysis, Nicolas Menguy for help with TEM characterization, Jacques Louis for assistance with XRD experiments, and Valentin Meunier for help with ICP-MS analysis.

REFERENCES

(1) Karapinar, D.; Creissen, C. E.; Rivera de la Cruz, J. G.; Schreiber, M. W.; Fontecave, M. Electrochemical CO_2 Reduction to Ethanol with Copper-Based Catalysts. *ACS Energy Lett.* **2021**, *6*, 694−706.

(2) Creissen, C. E.; Fontecave, M. Solar-Driven Electrochemical CO_2 Reduction with Heterogeneous Catalysts. *Adv. Energy Mater.* **2021**, *11*, 2002652.

(3) García de Arquer, F. P.; Dinh, C. T.; Ozden, A.; Wicks, J.; McCallum, C.; Kirmani, A. R.; Nam, D. H.; Gabardo, C.; Seifitokaldani, A.; Wang, X.; Li, Y. C.; Li, F.; Edwards, J.; Richter, L. J.; Thorpe, S. J.; Sinton, D.; Sargent, E. H. CO_2 Electrolysis to Multicarbon Products at Activities Greater than 1 A cm^{-2}. *Science* **2020**, *367* (6478), 661−666.

(4) Creissen, C. E.; Rivera de la Cruz, J. G.; Karapinar, D.; Taverna, D.; Schreiber, M. W.; Fontecave, M. Molecular Inhibition for Selective CO_2 Conversion. *Angew. Chem., Int. Ed.* **2022**, *61*, No. e202206279.

(5) Lv, J.-J.; Jouny, M.; Luc, W.; Zhu, W.; Zhu, J.-J.; Jiao, F.; Lv, J.; Jouny, M.; Luc, W.; Zhu, W. L.; Jiao, F.; Zhu, J. A Highly Porous Copper Electrocatalyst for Carbon Dioxide Reduction. *Adv. Mater.* **2018**, *30* (49), 1803111.

(6) Wang, R.; Haspel, H.; Pustovarenko, A.; Dikhtiarenko, A.; Russkikh, A.; Shterk, G.; Osadchii, D.; Ould-Chikh, S.; Ma, M.; Smith, W. A.; Takanabe, K.; Kapteijn, F.; Gascon, J. Maximizing Ag Utilization in High-Rate CO_2 Electrochemical Reduction with a Coordination Polymer-Mediated Gas Diffusion Electrode. *ACS Energy Lett.* **2019**, *4* (8), 2024−2031.

(7) Ma, S.; Sadakiyo, M.; Luo, R.; Heima, M.; Yamauchi, M.; Kenis, P. J. A. One-Step Electrosynthesis of Ethylene and Ethanol from CO_2 in an Alkaline Electrolyzer. *J. Power Sources* **2016**, *301*, 219−228.

(8) Rabinowitz, J. A.; Kanan, M. W. The Future of Low-Temperature Carbon Dioxide Electrolysis Depends on Solving One Basic Problem. *Nat. Commun.* **2020**, *11*, 5231.

(9) Ma, M.; Clark, E. L.; Therkildsen, K. T.; Dalsgaard, S.; Chorkendorff, I.; Seger, B. Insights into the Carbon Balance for CO_2 Electroreduction on Cu Using Gas Diffusion Electrode Reactor Designs. *Energy Environ. Sci.* **2020**, *13* (3), 977−985.

(10) Ozden, A.; Wang, Y.; Li, F.; Luo, M.; Sisler, J.; Thevenon, A.; Rosas-Hernández, A.; Burdyny, T.; Lum, Y.; Yadegari, H.; Agapie, T.; Peters, J. C.; Sargent, E. H.; Sinton, D. Cascade CO_2 Electroreduction

Enables Efficient Carbonate-Free Production of Ethylene. *Joule* **2021**, *5* (3), 706–719.

(11) Huang, J. E.; Li, F.; Ozden, A.; Rasouli, A. S.; de Arquer, F. P. G.; Liu, S.; Zhang, S.; Luo, M.; Wang, X.; Lum, Y.; Xu, Y.; Bertens, K.; Miao, R. K.; Dinh, C. T.; Sinton, D.; Sargent, E. H. CO_2 Electrolysis to Multicarbon Products in Strong Acid. *Science* **2021**, *372* (6546), 1074–1078.

(12) Xie, Y.; Ou, P.; Wang, X.; Xu, Z.; Li, Y. C.; Wang, Z.; Huang, J. E.; Wicks, J.; McCallum, C.; Wang, N.; Wang, Y.; Chen, T.; Lo, B. T. W.; Sinton, D.; Yu, J. C.; Wang, Y.; Sargent, E. H. High Carbon Utilization in CO2 Reduction to Multi-Carbon Products in Acidic Media. *Nat. Catal.* **2022**, *5* (6), 564–570.

(13) Gu, J.; Liu, S.; Ni, W.; Ren, W.; Haussener, S.; Hu, X. Modulating Electric Field Distribution by Alkali Cations for CO_2 Electroreduction in Strongly Acidic Medium. *Nat. Catal.* **2022**, *5* (4), 268–276.

(14) Yang, K.; Kas, R.; Smith, W. A. In Situ Infrared Spectroscopy Reveals Persistent Alkalinity near Electrode Surfaces during CO_2 Electroreduction. *J. Am. Chem. Soc.* **2019**, *141* (40), 15891–15900.

(15) Ehlers, J. C.; Feidenhans'l, A. A.; Kasper; Therkildsen, T.; Larrazábal, G. O. Affordable Green Hydrogen from Alkaline Water Electrolysis: Key Research Needs from an Industrial Perspective. *ACS Energy Lett.* **2023**, *8*, 1502–1509.

(16) Vermaas, D. A.; Smith, W. A. Synergistic Electrochemical CO_2 Reduction and Water Oxidation with a Bipolar Membrane. *ACS Energy Lett.* **2016**, *1* (6), 1143–1148.

(17) Peugeot, A.; Creissen, C. E.; Schreiber, M. W.; Fontecave, M. Advancing the Anode Compartment for Energy Efficient CO_2 Reduction at Neutral pH. *ChemElectroChem.* **2021**, *8* (14), 2726–2736.

(18) Yan, Z.; Hitt, J. L.; Zeng, Z.; Hickner, M. A.; Mallouk, T. E. Improving the Efficiency of CO_2 Electrolysis by Using a Bipolar Membrane with a Weak-Acid Cation Exchange Layer. *Nat. Chem.* **2021**, *13* (1), 33–40.

(19) Xie, K.; Miao, R. K.; Ozden, A.; Liu, S.; Chen, Z.; Dinh, C.-T.; Huang, J. E.; Xu, Q.; Gabardo, C. M.; Lee, G.; Edwards, J. P.; O'Brien, C. P.; Boettcher, S. W.; Sinton, D.; Sargent, E. H. Bipolar Membrane Electrolyzers Enable High Single-Pass CO_2 Electroreduction to Multicarbon Products. *Nat. Commun.* **2022**, *13* (1), 3609.

(20) Ma, M.; Kim, S.; Chorkendorff, I.; Seger, B. Role of Ion-Selective Membranes in the Carbon Balance for CO2 Electroreduction via Gas Diffusion Electrode Reactor Designs. *Chem. Sci.* **2020**, *11* (33), 8854–8861.

(21) Yang, K.; Li, M.; Subramanian, S.; Blommaert, M. A.; Smith, W. A.; Burdyny, T. Cation-Driven Increases of CO_2 Utilization in a Bipolar Membrane Electrode Assembly for CO_2 Electrolysis. *ACS Energy Lett.* **2021**, *6* (12), 4291–4298.

(22) Siritanaratkul, B.; Forster, M.; Greenwell, F.; Sharma, P. K.; Yu, E. H.; Cowan, A. J. Zero-Gap Bipolar Membrane Electrolyzer for Carbon Dioxide Reduction Using Acid-Tolerant Molecular Electrocatalysts. *J. Am. Chem. Soc.* **2022**, *144* (17), 7551–7556.

(23) Vass, A.; Endrodi, B.; Samu, G. F.; Balog, A.; Kormanyos, A.; Cherevko, S.; Janaky, C. Local Chemical Environment Governs Anode Processes in CO_2 Electrolyzers. *ACS Energy Lett.* **2021**, *6* (11), 3801–3808.

(24) Hong, Z.-S.; Cao, Y.; Deng, J.-F. A Convenient Alcohothermal Approach for Low Temperature Synthesis of CuO Nanoparticles. *Mater. Lett.* **2002**, *52* (1–2), 34–38.

(25) Monteiro, M. C. O.; Dattila, F.; Hagedoorn, B.; García-Muelas, R.; López, N.; Koper, M. T. M. Absence of CO_2 Electroreduction on Copper, Gold and Silver Electrodes without Metal Cations in Solution. *Nat. Catal.* **2021**, *4* (8), 654–662.

(26) Monteiro, M. C. O.; Philips, M. F.; Schouten, K. J. P.; Koper, M. T. M. Efficiency and Selectivity of CO_2 Reduction to CO on Gold Gas Diffusion Electrodes in Acidic Media. *Nat. Commun.* **2021**, *12* (1), 1–7.

(27) Todorova, T. K.; Schreiber, M. W.; Fontecave, M. Mechanistic Understanding of CO_2 Reduction Reaction (CO_2RR) Toward Multicarbon Products by Heterogeneous Copper-Based Catalysts. *ACS Catal.* **2020**, *10* (3), 1754–1768.

(28) Hawks, S. A.; Ehlinger, V. M.; Moore, T.; Duoss, E. B.; Beck, V. A.; Weber, A. Z.; Baker, S. E. Analyzing Production Rate and Carbon Utilization Trade-Offs in CO_2RR Electrolyzers. *ACS Energy Lett.* **2022**, *7* (8), 2685–2693.

(29) O'Brien, C. P.; Miao, R. K.; Liu, S.; Xu, Y.; Lee, G.; Robb, A.; Huang, J. E.; Xie, K.; Bertens, K.; Gabardo, C. M.; Edwards, J. P.; Dinh, C. T.; Sargent, E. H.; Sinton, D. Single Pass CO_2 Conversion Exceeding 85% in the Electrosynthesis of Multicarbon Products via Local CO_2 Regeneration. *ACS Energy Lett.* **2021**, *6*, 2952–2959.

(30) Gabardo, C. M.; O'Brien, C. P.; Edwards, J. P.; McCallum, C.; Xu, Y.; Dinh, C. T.; Li, J.; Sargent, E. H.; Sinton, D. Continuous Carbon Dioxide Electroreduction to Concentrated Multi-Carbon Products Using a Membrane Electrode Assembly. *Joule* **2019**, *3* (11), 2777–2791.

(31) Strathmann, H.; Rapp, H. J.; Bauer, B.; Bell, C. M. Theoretical and Practical Aspects of Preparing Bipolar Membranes. *Desalination* **1993**, *90* (1–3), 303–323.

(32) Pärnamäe, R.; Mareev, S.; Nikonenko, V.; Melnikov, S.; Sheldeshov, N.; Zabolotskii, V.; Hamelers, H. V. M.; Tedesco, M. Bipolar Membranes: A Review on Principles, Latest Developments, and Applications. *J. Membr. Sci.* **2021**, *617*, 118538.

(33) Chen, L.; Xu, Q.; Oener, S. Z.; Fabrizio, K.; Boettcher, S. W. Design Principles for Water Dissociation Catalysts in High-Performance Bipolar Membranes. *Nat. Commun. 2022 131* **2022**, *13* (1), 1–10.

(34) Oener, S. Z.; Foster, M. J.; Boettcher, S. W. Accelerating Water Dissociation in Bipolar Membranes and for Electrocatalysis. *Science* **2020**, *369* (6507), 1099–1103.

(35) Alerte, T.; Edwards, J. P.; Gabardo, C. M.; O'Brien, C. P.; Gaona, A.; Wicks, J.; Obradović, A.; Sarkar, A.; Jaffer, S. A.; Maclean, H. L.; Sinton, D.; Sargent, E. H. Downstream of the CO_2 Electrolyzer: Assessing the Energy Intensity of Product Separation. *ACS Energy Lett.* **2021**, *6* (12), 4405–4412.